

# Effect of Sintering Parameters and Powder Characteristics on the Performance of Metal-Injection-Molded SKD11 Parts

Huan–Xi Chen, You–Tern Tsai, and Kuan–Hong Lin

**Abstract**—Metal-injection-molded parts were fabricated using three kinds of SKD11 powder under different sintering parameters and with different binders and additives. An analysis of the microstructures and mechanical properties of these metal-injection-molded parts revealed that the porosity decreased and the grain size increased when the sintering isothermal holding increased. The average grain size was smaller for the part made of gas-atomized powder than for that made of water-atomized powder under the same sintering condition. The microstructures consisted of (Fe,Cr) solid solution substrates and Cr<sub>7</sub>C<sub>3</sub> carbide precipitates for the sintered part. For the specimen containing 10 wt % Fe, the mechanical property decreased due to less chromium carbide precipitates. The wear resistance and hardness of the sintered part made of gas-atomized powder were superior to those of the part made of water-atomized powder. In the pin-on-disk wear test, adhesive wear and a lower friction force were observed on the specimen with a lower hardness value. On the other hand, abrasive wear and a higher friction force were found for the specimen with a higher hardness value.

**Index Terms**—metal-injection-molded, microstructure, mechanical properties, SKD11

## I. INTRODUCTION

THE primary advantage of metal injection molding (MIM) is the elimination of a nonhomogeneous microstructure, better mechanical performance, easier formation of thinner parts, and better dimension control than achievable with traditional powder metallurgy and the press-forming process. MIM technology is suitable for fabricating small components that have complicated shapes. It has been widely applied in electronic components, vehicle parts, medical equipments, and military weapons [1].

The metallic powder size used in the MIM process is around 10 μm, comparatively smaller than that employed in traditional powder metallurgy. Therefore, better sintering performance and higher than 95% component density were achieved [1,2]. The metallic powder usually used in the MIM process consists of gas-atomized and water-atomized

powder. Gas-atomized powder shows superior performance in terms of filling and compaction but inferior shaping. On the other hand, water-atomized powder exhibits inferior filling and compaction but superior shaping due to its irregular shape.

For the purpose of increasing the filling of metallic powder at the injection stage, >40 vol % of binder was added into the feedstock of MIM. The binder usually has three components: a backbone polymer that provides strength, a filler phase that is easily extracted in the debinding, and a surfactant to bridge between the binder and the powder. The requirements of the binder include prevention of a chemical reaction with the metallic powder, prohibition of die and equipment corrosion, and easy debinding before the sintering process [1,3].

The carbon content of the SKD11 (AISI D2) alloy is around 1.4–1.6 wt %, and the primary alloying elements are chromium (11–13 wt %), vanadium (0.2–0.5 wt %), and molybdenum (0.8–1.2 wt %). The higher hardness value, toughness, and good wear-resistance performance of SKD11 made it popular and widely applied on various key parts and tools. This study was carried out to evaluate the three kinds of SKD11 powder. The sintering parameters, binders, and additives on the microstructure and mechanical properties of the metal-injection-molded SKD11 part were estimated.

## II. EXPERIMENTAL PROCEDURE

The metal powder used in this study was from three different vendors of SKD 11 (AISI D2) powder, usually chosen by the MIM manufacturer. There were two kinds of water-atomized powder (Mitsubishi UHT 10 and Atmix PF-20F) and one type of gas-atomized powder (Sandvik Osprey SKD11). A solid loading of metal powder was maintained at 56 vol %. The binder was composed of polypropylene, paraffin wax, ethylene vinyl acetate, stearic acid, carnauba wax, and polystyrene.

SKD11 powder was first blended with the binder, granulated, and then injection-molded. The green compacts underwent solvent debinding for 5 h, and they were subsequently sintered using a vacuum furnace. The thermal profile was heated at 1°C/min to 550°C, held for 60 min for the first stage of thermal debinding, and then heated at 3°C/min to 970°C, held for 60 min as the secondary stage of thermal debinding. This schedule was followed directly by heating at 4°C/min to 1100°C, held for 60 min, and then heating at 1°C/min to 1235°C, held for 60 or 150 min. All of the specimens were furnace-cooled.

The designation numbers of specimen, the composition of

Manuscript received Jan. 26, 2013; revised Feb. 13, 2013. This work was supported by the National Science Council of the Republic of China under Contract No. NSC 101–2221–E–236–003.

Huan–Xi Chen is with the Department of Mechanical Engineering, Tunghnan University, New Taipei City 222, Taiwan.

You–Tern Tsai is with the Department of Mechanical Engineering, De Lin Institute of Technology, New Taipei City 236, Taiwan.

Kuan–Hong Lin is with the Department of Mechanical Engineering, Tunghnan University, New Taipei City 222, Taiwan. (phone: 886-2-8662-5917; fax: 886-2-8662-5919; e-mail: khlin@mail.tnu.edu.tw).

the binders, the extra element added in the specimen, and the isothermal holding in sintering are listed in Table 1. The specimen designated as M was composed of water-atomized powder (Mitsubishi) with an average particle size of 9.5  $\mu\text{m}$ . The specimen designated as S was made of gas-atomized powder (Sandvik Osprey) with an average particle size of 10.1  $\mu\text{m}$ . On the other hand, the specimen designated as A consisted of gas-atomized powder (Atmix) with an average particle size of 10.4  $\mu\text{m}$ . AC indicates that the binder added carnauba wax, and AF indicates alloying 10% of Fe.

TABLE I  
DESIGNATION AND COMPOSITION OF SPECIMENS

Specimen designation	Binder (vol %)						Fe (wt %)	Isothermal holding (min)
	P.P.	P.W.	EVA	S.A.	C.W.	P.S.		
M60	38.1	42.1	8.2	3.5	8.1			60
M150	38.1	42.1	8.2	3.5	8.1			150
S150	35.9	52.7	8.5	2.9				150
A150	35.9	52.7	8.5	2.9				150
AC60	38.1	42.1	8.2	3.5	8.1			60
AC150	38.1	42.1	8.2	3.5	8.1			150
AF60	38.2	52.7		2.9		6.2	10	60
AF150	38.2	52.7		2.9		6.2	10	150

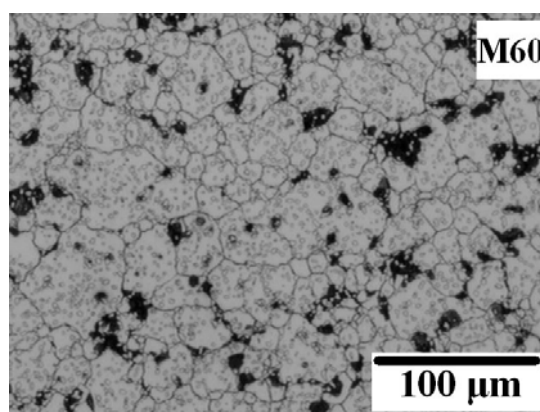
An etching reagent consisting of 3 vol % nitric acid and 97 vol % ethanol was used to etch the specimens for 10–60 s for the optical metallography examination. A scanning electron microscope (SEM) (TESCAM, 5136 LS) with an operating voltage of 15 kV was used to inspect the specimen after the wear test. The crystal structure of the specimen was analyzed using an X-ray diffractometer (Shimadzu, XRD-6000) at 30 kV and 30 mA with  $\text{CuK}\alpha$  ( $\lambda=0.15418$  nm) radiation. The scanning range ( $2\theta$ ) was set from  $20^\circ$  to  $80^\circ$  with a scan rate of  $5^\circ/\text{min}$ . A micro-hardness tester (Mitutoyo, HM-221) was used to determine the Vickers hardness (HV) of specimens. For this test, a 19.6 N load was applied, and 20 measurements were taken for averaging for each specimen. Pin-on-disk wear tests were carried out under dry sliding conditions in air. The SKD11 pin was used in the test, whereas the disk was made of high-speed steel (SKH9, HV 719) that rotated at a speed of 300 rpm under a normal load of 19.6 N for 120 min.

### III. RESULTS AND DISCUSSION

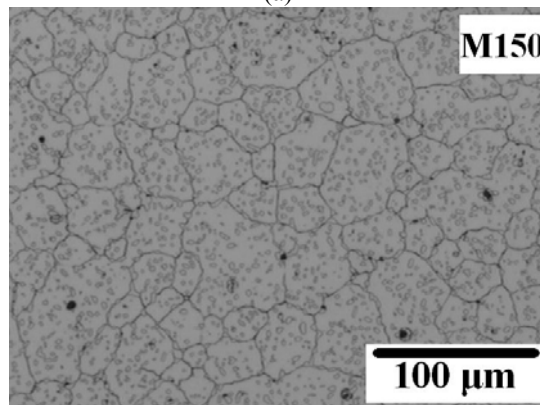
#### A. Microstructure

The M60 and M150 specimens had the same binder and sintering temperature of  $1235^\circ\text{C}$  but different isothermal holdings for 60 or 150 min, respectively. Figure 1(a) shows the optical photomicrograph of the M60 specimen. Several large pores and undensification microstructures were observed due to insufficient isothermal holding at the sintering temperature. The average grain size was around 22  $\mu\text{m}$ . Figure 1(b) shows the optical photomicrographs of the M150 specimen. A few micro pores in the microstructure were observed; the average grain size was around 29  $\mu\text{m}$ . A lot of irregular shapes and tiny precipitated phases inside the grains were inspected in both specimens.

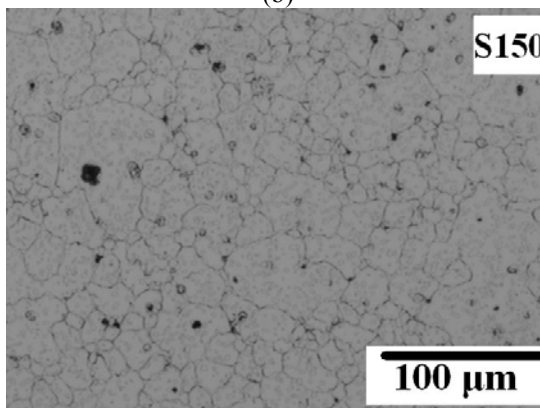
The S150 and A150 specimens were made of water-atomized and gas-atomized powder with average particle sizes of 10.1 and 10.4  $\mu\text{m}$ , respectively. The same binder composition, sintering temperature, and isothermal holding were chosen for both specimens.



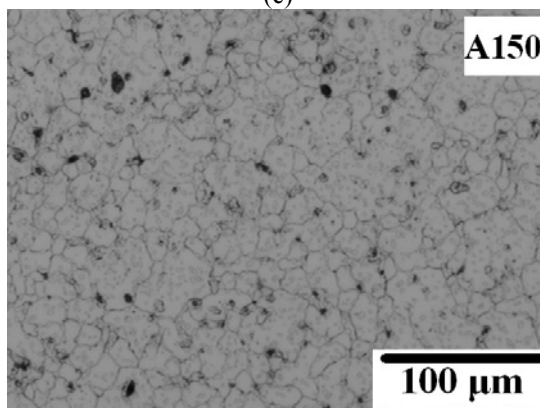
(a)



(b)



(c)



(d)

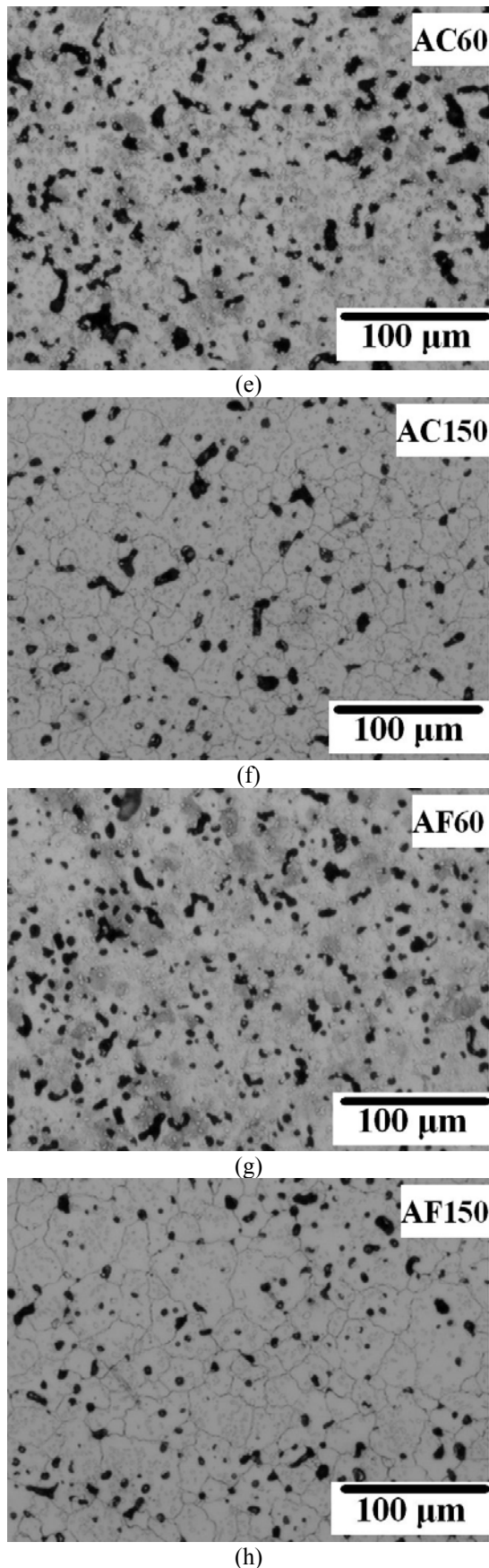


Fig. 1. Optical photomicrographs of sintered specimens: (a) M60, (b) M150, (c) S150, (d) A150, (e) AC60, (f) AC150, (g) AF60, and (h) AF150.

Figures 1(c) and 1(d) show the optical photomicrographs of both specimens. The number of pores inside the microstructure of the A150 specimen slightly exceeded that in the S150 specimen; however, the size of most pores was

smaller than 5 µm. The average grain sizes of the S150 and A150 specimens were around 26 and 27 µm, respectively. Furthermore, a large number of irregular shapes and tiny precipitated phases inside the grains were observed in both specimens.

The AC60 and AC150 specimens were made using the same metal powder, binder, and sintering temperature (1235°C) but different isothermal holdings for 60 and 150 min, respectively. Figures 1(e) and 1(f) show the optical photomicrographs of both specimens. The AC60 microstructure has a higher number of pores than the AC150 specimen. In addition, the amount and size of the precipitated phase of the AC60 and AC150 specimens were almost the same. For this reason, the precipitated phase should be formed during the furnace cooling stage and have no relation to the sintering isothermal hold.

It could also be seen that the AC150 microstructure has more pores than the A150 specimen, even though the same isothermal holding was chosen for both specimens. A binder used for A150 was composed of P.P., P.W., EVA, and S.A.; these components were also used in the binder for the AC150 specimen, along with the extra addition of carnauba wax. In this study, a binder composition without added carnauba wax provided a denser microstructure than a binder including the wax.

The identical binder composition and nearly identical average particle sizes for the M150 and AC150 specimens are notable. A few small pores in the microstructure of the M150 specimen were noted. However, many large pores were observed in the AC150 specimen. It can be concluded that not only the binder compositions but also the vendor of the powders used affected the microstructure of the specimens in this study.

Extra 10 wt % Fe was added to the composition of the AF60 and AF150 specimens, which were sintered at 1235°C with isothermal holdings for 60 or 150 min, respectively. Figures 1(g) and 1(h) show the optical photomicrograph of the AF60 and AF150 specimens. The number of pores in the AF60 and AF150 microstructures was very similar to that of the AC60 and AC150 specimens, except that the pore size of AF150 was smaller than that of AC150.

Figure 2 shows that the number of precipitated phases of AF150 was slightly less than that of A150, which was possibly due to the 10 wt % of Fe added into AF150, thus decreasing the proportion of the SKD11 alloy powder and accordingly decreasing the number of carbide-precipitation phases. It was often observed that the coarsen carbide precipitated at the grain boundary of Fe-Cr alloy and decreased the carbon and chromium content in the grain, thus causing brittleness and weakening the alloy [4]. Because the appropriate sintering parameters were selected in this study, the carbides precipitated inside the grains, consequently enhancing the mechanical properties of the component.

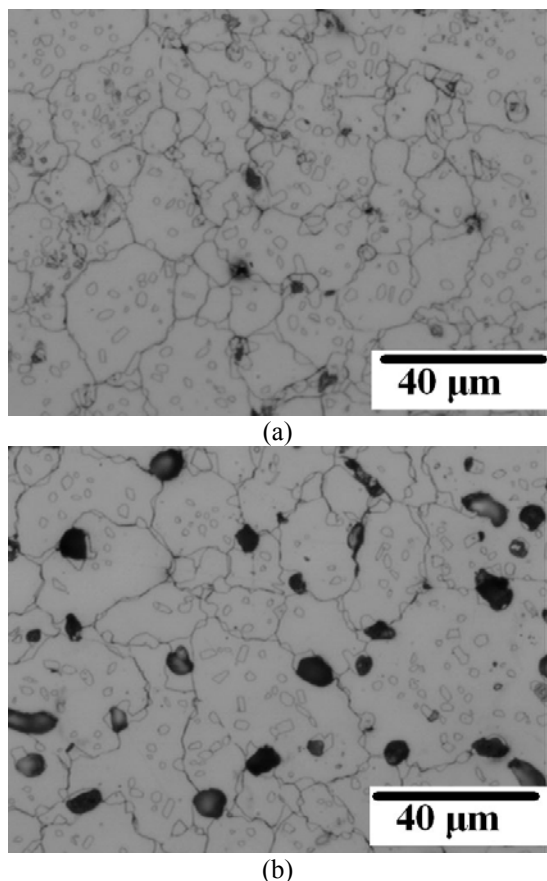


Fig. 2. Optical photomicrographs of sintered specimens: (a) A150 and (b) AF150.

### B. X-ray diffraction analysis

Figure 3 displays the X-ray diffraction (XRD) pattern of the AC150 specimen. It is evident that the matrix of the sintered component is a (Fe,Cr) solid solution (JCPDS 65-7775) with a cubic crystal structure. The average lattice constant of the crystal is 0.2873 nm. The precipitated phase is Cr<sub>7</sub>C<sub>3</sub> (JCPDS 65-1347) [4]. Although other researchers have previously reported some precipitated carbides, such as M<sub>3</sub>C<sub>2</sub>, M<sub>23</sub>C<sub>6</sub>, and M<sub>2</sub>C, in the SKD11 alloy [5], no apparent corresponding diffraction pattern was observed in the present analysis.

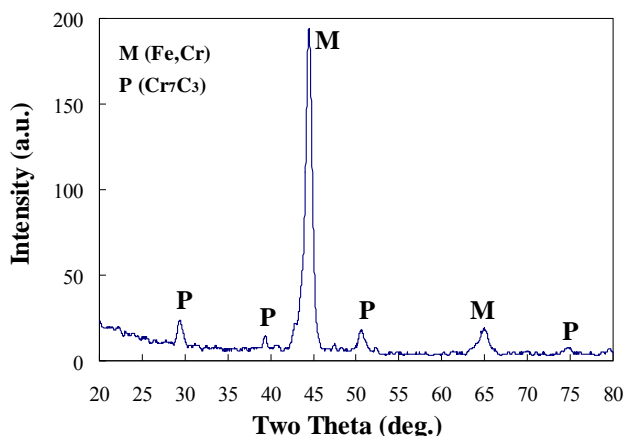


Fig. 3. X-ray diffraction pattern of the AC150 specimen.

### C. Mechanical properties

#### Hardness

Table 2 shows the Vickers hardness (mHV) of various specimens. Increased isothermal holding resulted in higher surface hardness for the specimens. Comparing all the specimens with the same isothermal holding of 150 min, the average surface hardness values of the specimens were M150 (mHV 784, water-atomized powder), S150 (mHV 723, gas-atomized powder), A150 (mHV 655, water-atomized powder), AF150 (mHV 585, water-atomized powder), and AC150 (mHV 531, water-atomized powder). The results also indicate that the hardness of specimens was associated with microstructures. The microstructure had a small grain, a few pores, and more carbide-precipitation phases that provide higher hardness. All the specimens in this study were as-sintered; a suitable heat-treatment procedure will increase these specimens' mechanical properties [6].

TABLE II  
SURFACE HARDNESS, WEIGHT LOSS, AND FRICTION FORCE OF THE VARIOUS SINTERED SPECIMENS

Designation	Isothermal holding (min)	Hardness (mHV)	Weight loss (10 <sup>-4</sup> g)	Friction force (N)
M60	60	545	7	24
M150	150	784	3	25
S150	150	723	3	25
A150	150	655	4	26
AC60	60	244	18	19
AC150	150	531	6	25
AF60	60	319	15	21
AF150	150	585	5	23

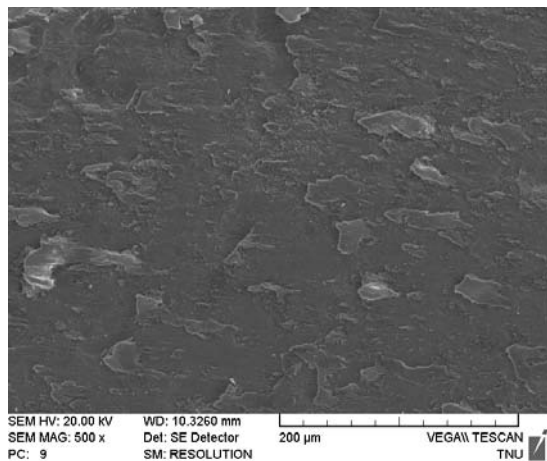
#### Wear test

Figures 4(a) and 4(b) show the SEM image of the M60 and M150 specimens after 120 min of a pin-on-disk wear test. The adhesive wear characteristic was observed in the M60 specimen. Because the metal adhesion and shear phenomena occurred continually between the specimen and the disk, a large variation of friction force was observed in a wear test curve, as shown in Fig. 5 [7].

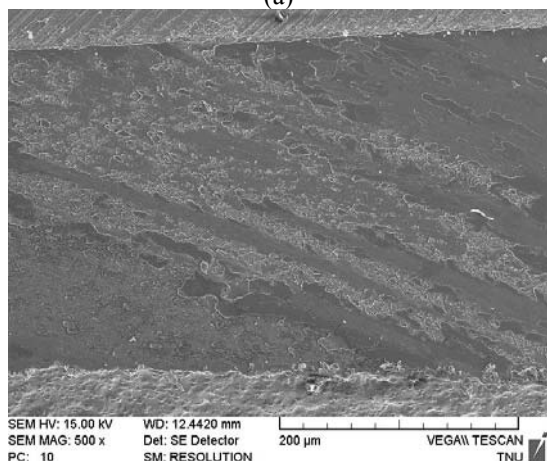
The abrasive wear and a part of the adhesive wear were observed in the M150 specimen. Abrasive wear usually occurred between two materials with highest hardness values. The M150 specimen (mHV 784) and the SKH9 disk (mHV 719) had the highest hardness indices and had the abrasive wear type. The average friction forces of the M60 and M150 specimens were 24 and 25 N, respectively.

The wear type of the S150 and A150 specimens were similar to that of M150. Both adhesive wear and abrasive wear were also observed. The average friction forces of the S150 and A150 specimens were 25 and 26 N, respectively.

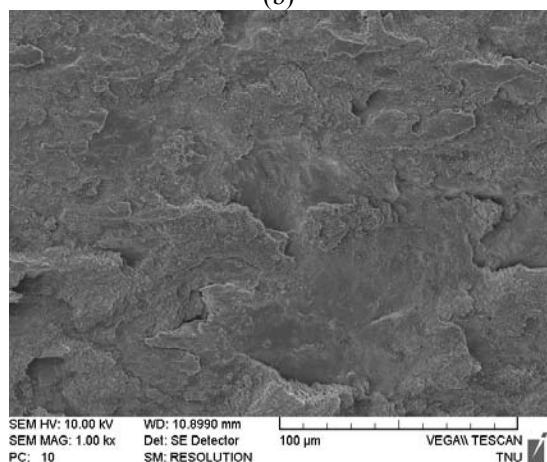
The average friction force of specimens AC60 was 19 N. A serious ductile tear phenomenon on the surface was observed after the wear test due to the lowest hardness value of the AC60 specimen. The wear type of the AC150 specimen was also similar to that of M150. However, the hardness value of AC150 was lower than that of M150. Consequently, a higher proportion of the adhesive wear was observed. The average friction force of the AC150 specimen was 25 N. Based on the above observations, it can be concluded that a specimen with a low hardness value in contact with high-speed steel triggers a lower friction force and that one with a high hardness value is prone to a higher friction force.



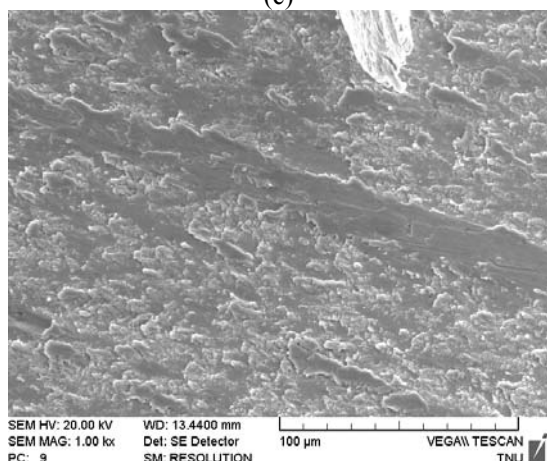
(a)



(b)



(c)



(d)

Fig. 4. SEM image of specimens: (a) M60, (b) M150, (c) AC60, and (d) AC150 after 120 min of the pin-on-disk wear test.

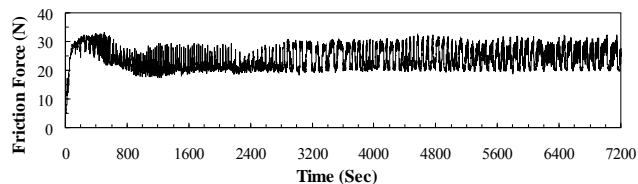


Fig. 5. The pin-on-disk wear test result of the M60 specimen.

Table 2 shows the weight loss of whole specimens after wear tests. The AC60 specimen had the lowest surface hardness (mHV 244) and thus the highest weight loss ( $18 \times 10^{-4}$  g), with the AF60 specimen following ( $15 \times 10^{-4}$  g). On the other hand, the M150 specimen had the highest surface hardness (mHV 784) and therefore the lowest weight loss ( $3 \times 10^{-4}$  g). The weight loss of specimens was not completely inversely proportional to the surface hardness though, which may be the result of an experiment error in this study. The M150 and S150 specimens had superior hardness and wear-resistance performance because they had fewer pores, a smaller grain size, and plenty of precipitated carbide in their microstructures [4,7]. Compared with the A150 specimen, AF150 had additional 10 wt % of iron in the SKD11 alloy to save on powder cost. However, it slightly decreased hardness values and increased weight loss after the wear test.

#### IV. CONCLUSION

An increase in isothermal holding resulted not only in a decrease in pores but also in a densification of the structure of the SKD11 alloy. However, the grain size slightly increased simultaneously. The matrix of the SKD11 sintered specimen is the (Fe,Cr) solid solution, and the precipitated phase is  $Cr_7C_3$ . The sintered specimen made of gas-atomized powder had a smaller average grain size, fewer pores, and a higher hardness index compared with the water-atomized powder specimen at identical sintering parameters. Superior wear-resistance performance was also observed. An addition of 10 wt % of iron in the SKD11 powder can save costs, but it can also increase the pores and decrease the carbide-precipitation phases in the microstructure, leading to the worsening of mechanical properties.

#### REFERENCE

- [1] R.M. German and A. Bose, "Injection Molding of Metals and Ceramics (Book style). Metal powder industries federation. New Jersey. 1997, pp. 11–24.
- [2] R.M. German, *Powder Metallurgy Science* (Book style). Metal powder industries federation. New Jersey. 1994, pp. 192–201.
- [3] Y. L. Fan and K. S. Hwang, "Properties of metal injection molded products using titanate-containing binders", *Materials Transactions*, vol. 48, no. 3, pp. 544–49, 2007.
- [4] K. H. Lin, Y. X. Sun, G. L. Chen, K. M. Lin and Y. C. Hsieh, "Effect of sintering temperature on the microstructure and mechanical properties of MIM SKD11 component", *Advances in Powder Metallurgy & Particulate Materials*, part 4, p.1320, 2011.
- [5] A. Tiziani and A. Molinari, "Improvement of AISI D2 steel properties by unconventional vacuum heat treatments, *Materials Science and Engineering: A*, vol. 101, pp. 125–133, 1988.
- [6] K. H. Lin, Y. C. Hsieh and S. T. Lin, Microstructure and mechanical performance analysis of metal-injection-molded Fe-2Ni sintered components, *American Institute of Physics*, vol. 1315, pp.707–12, 2010.

- [7] K. H. Lin, "Wear behavior and mechanical performance of metal injection molded Fe-2Ni sintered components", *Materials and Design*, vol. 32, no.3, pp. 1273-82, 2010.